Impaired Th1/Tc1 Cytokine Production of Tumor-Infiltrating Lymphocytes in a Model of Primary Intraocular B-Cell Lymphoma

Valérie Touitou,[1] Cécile Daussy,[1] Bahram Bodaghi,[2] Serge Camelo,[3] Yvonne de Kozak,[3] Phuc Lehoang,[2] Marie-Christine Naud,[3] Audrey Varin,[1] Brigitte Thillaye-Goldenberg,[3] Hélène Merle-Béral,[4] Wolf Herman Fridman,[1] Catherine Sautès-Fridman,[1] and Sylvain Fisson[1]

Purpose. Primary intraocular lymphoma is a high-grade non-Hodgkin lymphoma with a pathogenesis that is still unclear. Microenvironment is known to be crucial in controlling tumor growth and maintenance. To study the immune microenvironment in intraocular lymphomas and to characterize the cytokine polarization of infiltrating T-lymphocytes, a new murine model of intraocular B-cell lymphoma was developed.

Methods. Immunocompetent adult mice were injected intravitreally with a syngeneic lymphomatous B-cell line. Clinical, histologic, and flow cytometric analyses were performed to characterize the tumoral invasion and the immune infiltration. Cytokine production of ocular cells was investigated by RT-PCR and fluorescent immunoassay, with or without stimulation by anti-CD3$^+$ anti-CD28 antibodies.

Results. Intraocular lymphoma developed in eyes injected by lymphomatous B-cells. At day 19, the retina and the vitreous cavity were infiltrated by tumor cells. Up to 15% of living cells were T-lymphocytes. Cytokine profile analysis of the supernatant of ocular cells cultured ex vivo demonstrated the presence of IL10, IL6, IFNγ, and TNFα. Stimulation of ocular cells with anti-CD3$^+$ anti-CD28 antibodies increased the IFNγ level and led to the induction of IL2 production, completing the type 1 (Th1/Tc1-like) pattern of cytokine expression observed. IL12p70 and IL4, potent Th1 or Th2 differentiating factors, were undetectable, even after stimulation.

Conclusions. The results suggest that T-cells from intraocular B-lymphomas are characterized by a Th1/Tc1-like profile that could be partially inhibited in vivo. These data raise the possibility of a T-cell immunostimulation to reactivate the Th1/Tc1-lymphocytes and improve intraocular antitumoral immunity. (*Invest Ophthalmol Vis Sci.* 2007;48:3223–3229) DOI: 10.1167/iovs.07-0008

Primary intraocular lymphoma (PIOL) is a subset of primary central nervous system lymphomas (PCNSLs), and its incidence has tripled over the past 15 years.[1] Data concerning the immune microenvironment of PIOLs are scarce due to the location of the tumor in the eye. Only a few cytopathological studies report the presence of T-cell infiltration in patients with intraocular B-cell lymphoma.[2]

Increasing evidence suggests that the immune system regulates cancer development by several mechanisms.[3,4] This regulation can be either beneficial through immunosurveillance[5,6] or detrimental by facilitating tumor progression in many ways, such as shaping the immunophenotype of tumors,[7–9] creating an immunosuppressive environment, or inducing regulatory T-cells.[10,11] In many cancers, anti-tumor T-cell responses have been characterized by a predominant polarization in either a helper T-cell type-1 (Th1) response, characterized by the production of IL-2, interferon (IFN)-γ, and tumor necrosis factor (TNF)-α, or a Th2-type response, characterized by the production of IL-4, -5, -10, and -13.[12–14] Defining the type of infiltrating T-lymphocyte (TIL) polarization in the tumor microenvironment can help in the comprehension of tumor progression[15] and is critical for the development of new therapeutic strategies.[16,17]

Few animal models are available for the study of intraocular lymphoma. The first two models of PIOL were obtained after injection of murine lymphomatous T-cells in immunocompetent newborn[18] or adult mice.[19] However, 84% to 98% of PIOLs are B-cell lymphomas,[1] which are expected to express major histocompatibility complex (MHC) class II and costimulatory molecules that play an important role in the induction of antitumor immune responses. Recently, a new xenogeneic model of intraocular B-cell lymphoma has been reported.[20] Although this model is a B-cell lymphoma, it has been developed in immunodeficient SCID mice, which limits the study of tumor microenvironment and of the antitumoral immune response due to an incompletely effective arm of immunity. We thus developed the first murine model of B-cell lymphoma in a syngeneic immunocompetent host, allowing the characterization of the immune infiltrate and the Th-type response.

From the [1]Immune Microenvironment and Tumors Group and [3]Physiopathology of Eye Diseases Group, INSERM (Institut National de la Santé et de la Recherche Médicale) UMRS872, Université Pierre et Marie Curie-Paris, Université René Descartes-Paris, Centre de Recherche des Cordeliers, Paris, France; and the Departments of [2]Ophthalmology and [4]Hematology Hôpital de la Pitié-Salpêtrière, Paris, France.

Supported by the Association pour la Recherche contre le Cancer, Institut National du Cancer Grant RC013-2005, the Institut National de la Santé et de la Recherche Médicale, the University Pierre and Marie Curie and the University René Descartes and the pole de compétitivité Ile de France (ImmuCan project). VT is a beneficiary of study grants from the Fédération des Aveugles de France and the Fondation de France (Fouassier). CD is a recipient of a grant from the Institut National du Cancer.

Submitted for publication January 4, 2007; revised February 26, 2007; accepted April 16, 2007.

Disclosure: **V. Touitou**, None; **C. Daussy**, None; **B. Bodaghi**, None; **S. Camelo**, None; **Y. de Kozak**, None; **P. Lehoang**, None; **M.-C. Naud**, None; **A. Varin**, None; **B. Thillaye-Goldenberg**, None; **H. Merle-Béral**, None; **W. Herman Fridman**, None; **C. Sautès-Fridman**, None; **S. Fisson**, None

The publication costs of this article were defrayed in part by page charge payment. This article must therefore be marked "*advertisement*" in accordance with 18 U.S.C. §1734 solely to indicate this fact.

Corresponding author: Sylvain Fisson, INSERM UMRS872 Immune Microenvironment and Tumors Group, Centre de Recherche des Cordeliers, IFR58, 15 rue de l'Ecole de Médecine, F-75006, Paris, France; sylvain.fisson@upmc.fr.

METHODS

Cell Line

IIA1.6 cells were derived from A20-2J murine B-cell lymphoma ($H2^d$).[21] Cells were grown in culture in RPMI medium (Glutamax; Invitrogen-Gibco, Cergy Pontoise, France), supplemented with 10% fetal calf serum (FCS; PAA Laboratories, Cölbe, Germany), penicillin 100 U/mL, and streptomycin 100 μg/mL (Eurobio, Les Ulis, France), sodium pyruvate 10 mM (Invitrogen-Gibco), and 2-mercaptoethanol 50 mM (Invitrogen-Gibco) and were maintained at 37°C with 5% CO_2.

Transfection

IIA1.6 cells were transfected by nucleofection, using a procedure, with a plasmidic construct of 3.5kb pmaxGFP (Amaxa Biosystems, Cologne, Germany), under control of the cytomegalovirus (CMV) promoter. When illuminated with a 488 nm Argon ion laser, the green fluorescent protein (GFP) emitted in the green channel at 510 nm and allowed the observation of the transfected cells in vivo. After transfection, the cells were cultivated in culture medium and selected with 0.5 mg/mL neomycin (G418). Clones expressing high levels of GFP were obtained by limit dilution.

Mice

Female BALB/c mice ($H2^d$), 6 to 10 weeks old, were obtained from Charles River Laboratories (L'Arbresle, France). Mice were provided with sterile food and filtrated water ad libitum and kept on a 12-hour light–dark cycle. All mice were manipulated according to European Union guidelines and the ARVO Statement for the Use of Animals in Ophthalmic and Vision Research.

Intravitreal Injections and Clinical Evaluation

Anesthesia was performed using intraperitoneal injection of a combination of 120 mg/kg ketamine (Imalgene1000; Merial, Lyon, France) and 6 mg/kg xylazine (Rompun 2%; Bayer, Leverkusen, Germany). Cells in 2 μL 1× phosphate-buffered saline (pH 7.4; PBS), were injected intravitreally through the pars plana with the aid of a dissecting microscope. Mice were injected in aseptic conditions in the right eye after dilatation with tropicamide 0.5% (Théa, Clermont-Ferrand, France), through a 32-gauge needle attached to a syringe (Hamilton; Hamilton Bonaduz AG, Bonaduz, Switzerland). Control mice were injected intravitreally with 2 μL PBS in the right eye. Rifamycin (Merck, Sharp & Dohme-Chibret, Clermont-Ferrand, France) drops were instilled after the injection. A slit lamp examination was performed weekly, including bilateral fundus examination in each mouse. Clinical progression was graded according to a clinical score of ocular involvement (Table 1). Mice were euthanatized by cervical dislocation.

TABLE 1. Slit Lamp-Based Ocular Clinical Scoring of Mice with PIOL

Location/Condition	Score
Anterior chamber	
No retrokeritic precipitates (RKP)	0
Granulomatous RKP	1
Confluent RKP	2
Iris infiltration	1
Vitreous	
No vitritis	0
Mild vitritis	1
Dense vitritis	2
Retina	
No infiltrates	0
Focal infiltrates	1
Diffuse infiltrates	2
Other features	
Vasculitis	0
Optic disc edema	1
Tumoral retinal detachment	2

Histology

After death, eyes were collected, postfixed in 4% paraformaldehyde containing 5% sucrose for 2 hours, and embedded in resin for fine histology according to the provider's instructions (Historesin embedding kit; Leica Microsystems, Heidelberg, Germany).[22] Serial sections (5 μm) were stained with toluidine blue. Microscopic examination of the eye sections was then performed (Leitz microscope; Aristoplan, Rueil-Malmaison, France). Images were collected (DFC480 Leica, with the software IM50 Image manager; Leica Microsystems).

Immunohistochemistry

The enucleated eyes were fixed in a solution containing 4% paraformaldehyde and 5% sucrose for 2-hours, then immersed overnight in PBS containing 15% sucrose. The samples were embedded and frozen in optimal cutting-temperature compound (Tissue-Tek; Sakura Finetek, Zoeterwoude, The Netherlands) and stored at −80°C. Frozen anteroposterior sections (10 μm thick) of eyes at the optic nerve level were cut with a cryostat (CM3050S; Leica, Wetzlar, Germany) and mounted on gelatin-coated slides for immunohistochemical analysis.[23] For immunostaining, the slides were incubated with purified rat monoclonal antibody (mAb) against murine T-cells (CD4 clone GK1.5, CD8 clone 53-6-7; BD Biosciences, Le Pont-de-Claix, France), macrophages (clone F4/80), and polymorphonuclear neutrophils (clone 7/4; Serotec, Cergy Saint-Christophe, France). Revelation was performed with Alexa594-conjugated anti-mouse antibody (Invitrogen-Gibco). In some experiments, the slides were incubated with the nuclear staining agent propidium iodide (Invitrogen-Molecular Probes, Eugene, OR). Negative control experiments were performed by incubation of the slides with isotype control mAb. The sections were mounted in PBS containing 50% glycerol and observed by fluorescence photomicroscopy (FXA, Microphot; Nikon, Melville, NY).

Confocal Microscopy and Image Analysis

Confocal microscopy was performed on the frozen eye sections with a laser scanning confocal microscope (LSM510; Carl Zeiss Meditec, GmbH, Oberkochen, Germany), equipped with an argon laser (488 nm) and a helium-neon laser (543 nm). The images were merged with image-browser software (LSM; Carl Zeiss Meditec, GmbH) to produce a composite multicolor image.

Flow Cytometry

The eyes were dissected in RPMI medium, digested with 0.1 mg/mL DNase I (Roche, Meylan, France) and 1.67 Wünch units/mL of purified enzymes (Liberase; Roche) at 37°C for 20 minutes, filtered, and rinsed in PBS with 2 mM EDTA and 3% FCS. Cells were preincubated with 2.4.G2 mAb (10 μg/mL) to block nonspecific binding to Fc receptors and then 10^5 cells per well were stained with the following mAbs: biotin-conjugated anti-CD3 (145-2C11; BD Biosciences), phycoerythrin-conjugated anti-CD4 (GK1.5; BD Biosciences), a fluorochrome (Cy-Chrome)–conjugated anti-CD8 (53-6.7; BD Biosciences), phycoerythrin-conjugated anti-CD19 (6D5; e-Bioscience, San Diego, CA) or the corresponding isotypic mAb control (BD Biosciences). The biotinylated mAbs were detected by allophycocyanin-conjugated streptavidin (BD Biosciences). Flow cytometry (FACSCalibur) analyses were performed with the accompanying software (CellQuest; BD Biosciences).

RNA Isolation and Quantification of Intraocular IL-10 mRNA Levels by RT-PCR

Total RNA was isolated from freshly enucleated eyes by the acid guanidinium thiocyanate-phenol-chloroform method.[24] In each sample, the concentration was readjusted according to the RNA optic density at 260 nm, and β-actin mRNA was transcribed and amplified in parallel. PCR fragments were analyzed by 3% agarose gel electrophoresis and visualized by ethidium bromide staining under UV. The relative

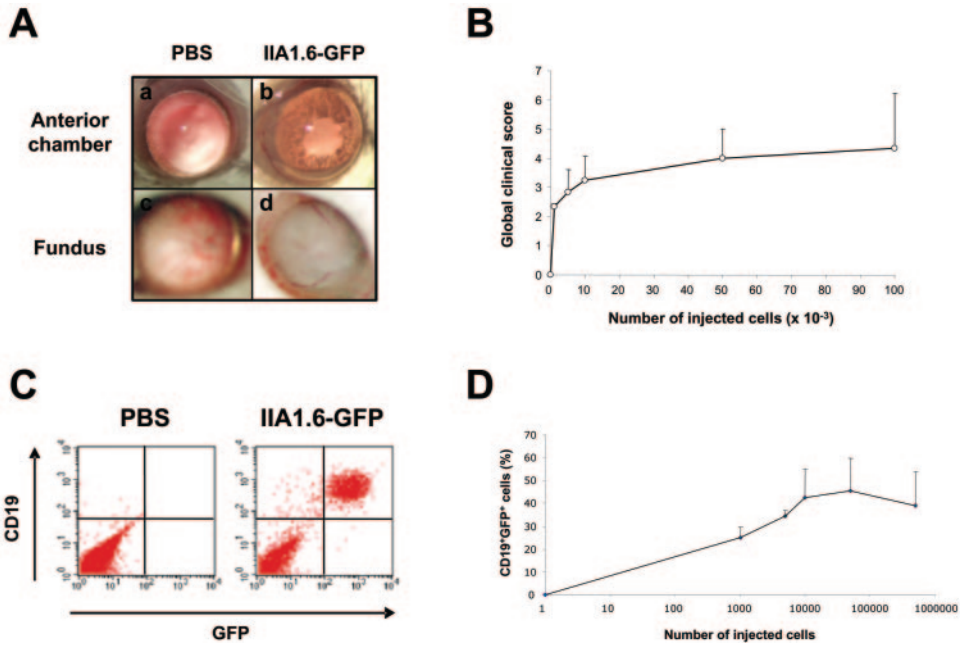

FIGURE 1. Development of intraocular lymphoma in eyes inoculated intravitreally with IIA1.6 murine B-cell lymphoma, compared with control eyes in a dose–response manner. Anterior chamber (**Aa**) and fundus (**Ac**) of a mouse injected with PBS in the right eye compared with the anterior chamber (**Ab**) and the posterior segment (**Ad**) of a mouse injected with IIA1.6-GFP murine lymphoma B-cells in the right eye. (**B**) Global clinical scoring performed after injection of an increasing number of cells in the right eyes. Clinical scoring was obtained on slit lamp examination of both eyes, with fundus examination of each mouse. Data are obtained from two independent experiments ($n = 6$) and standard deviations are represented. (**C**) Dot plot representation of flow cytometric analyses for tumor cell identification at day 12 after intravitreous inoculation of PBS (*left*) or IIA1.6-GFP cells (*right*). IIA1.6-GFP tumor cells were detected among living cells with double fluorescence due to GFP^+ and $CD19^+$ staining (*top right quadrant*). Shown are two representative dot plots of one experiment from three independent experiments performed. (**D**) Dose response assessed by flow cytometric analysis of tumoral eyes injected with an increasing number of tumor cells. All samples were harvested and analyzed at day 19 after injection. Data are obtained from two independent experiments ($n = 6$) and standard deviations are represented.

band intensity was calculated in comparison with β-actin. Sequences for β-actin forward and reverse primers (Sigma-Genosys, St. Quentin Fallavier, France), IL-10 forward and reverse primers (BD-Clontech Laboratories, Palo Alto, CA) were as follows: β-actin forward: GTG GGC CGC TCT AGG CAC CAA; β-actin reverse: CTC TTT GAT GTC ACG CAC GAT TTC; IL-10 forward: ATG CAG GAC TTT AAG GGT TAC TTG GGT T; and IL-10 reverse: ATT TCG GAG AGA GGT ACA AAC GAG GTT T. Primers were designed to amplify specifically the cDNA fragments representing mature mRNA transcripts of 539 bp for β-actin and 455 bp for IL-10. PCR amplifications were performed according to the manufacturer's instructions.

T-Cell Stimulation and Cytokine Detection

Cells ($n = 10^5$) isolated from injected eyes were stimulated by 5 μg/mL of anti-CD3ε and anti-CD28 mAbs (BD Biosciences) or by 100 ng/mL of lipopolysaccharide (LPS; Sigma-Aldrich, St. Quentin Fallavier, France) at 37°C. For cytokine detection, supernatants were collected after 36-hours and assayed for IL-2, IL-4, IL-6, IL-10, IL-12p70, IFNγ, TNFα, and granulocyte-macrophage–colony-stimulating factor (GM-CSF) by using a mouse bead array (Cytometric Bead Array Flex; BD Biosciences), according to the manufacturer's instructions.

RESULTS

Intraocular Development of a B-Cell Lymphoma on Intravitreal Injection of IIA1.6 Cells

To generate a murine model of intraocular lymphoma, normal immunocompetent BALB/c mice ($H2^d$) received an intravitreous injection of the syngeneic IIA1.6-GFP lymphoma B-cell line. The IIA1.6 cell line was transfected with the GFP to enable observation of tumor growth and to allow discrimination of lymphomatous B-cells from host normal B-cells. The mice were examined weekly by slit lamp, including fundus examination. An illustration of clinical involvement of the anterior chamber and retina is presented in Figure 1A and the global clinical score is shown in Figure 1B for each dose of cells injected. Anterior chamber invasion with keratic precipitates and flare, vitreous haze, and retinal infiltration were observed after day 7 if more than 5.10^4 cells were injected, but only after day 14 for mice injected with 10^4 or less cells. Vasculitis, optic disc edema, or retinal detachment was observed after day 21 in some mice. At this time, left eyes were clinically clear of malignant cells in all cases, and no neurologic sign was observed. The tumors continued to grow up to 3 months.

IIA1.6-GFP B-cells were detected by flow cytometric analysis in all inoculated eyes using the double detection of GFP and CD19 (Fig. 1C). The percentage of intraocular lymphomatous cells was correlated in a dose–response manner to the number of cells initially injected in right eyes at initial doses of fewer than 10^4 cells (Fig. 1D). Results were reproducible, with the development of intraocular lymphoma in all eyes injected with IIA1.6-GFP cells. At more than 10^4 cells injected initially, the percentage of tumor cells reached a plateau. Considering these results, we chose the dose of 10^4 cells injected intravitreally to induce intraocular lymphomas. No GFP^+CD19^+ cells were detected in the left, noninjected, eyes.

To determine the kinetics of tumor growth, mice were evaluated at days 7, 14, and 21 by slit lamp examination (Fig. 2A) and at days 6, 12, and 19 by flow cytometry (Fig. 2B). Clinically, vitreous and retinal invasion appeared at day 7 and increased progressively. Significant anterior chamber involvement with retrokeratic precipitates was observed beginning at day 14 (Fig. 2A). Similarly, at day 6, lymphomatous cells detected by flow cytometry represented 3% of ocular living cells and reached up to 40% at day 21 (Fig. 2B).

The ocular distribution of IIA1.6-GFP cells at day 12 was studied on resin-embedded and frozen sections. In the anterior segment, tumor cells were located along the corneal endothelium (Fig. 3A) and some of them infiltrated the iris (Fig. 3B) and the ciliary body epithelium (data not shown). IIA1.6-GFP cells progressively invaded and filled the whole anterior chamber (Fig. 3C). In the posterior segment, IIA1.6-GFP cells were

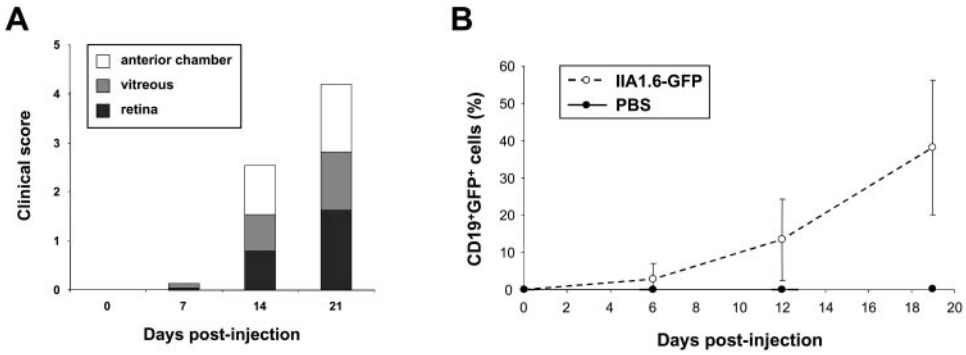

FIGURE 2. Kinetics of tumor growth in eyes injected with 10^4 IIA1.6-GFP lymphomatous B-cells. (**A**) Mean of clinical score at days 7, 14, and 21 for the different structures infiltrated clinically in the eyes of mice intravitreally injected with IIA1.6-GFP cells at day 0. Data are obtained from two independent experiments ($n = 6$). (**B**) Tumor growth at days 6, 12, and 19, determined by flow cytometric analysis as the percentage of $CD19^+GFP^+$ cells among living cells in the right eye injected at day 0 with PBS ($n = 23$) or 10^4 IIA1.6-GFP cells ($n = 26$). Data shown are from four independent experiments, and standard deviations are represented.

observed in the vitreous (Fig. 3D) and accumulated along the internal limiting membrane of the retina (Figs. 3E, 3F). At that time, the retina did not show any major architectural modification (Figs. 3E, 3F), except in focal areas, where invasion of tumor cells caused local alteration of the retinal organization (Fig. 3G). Tumor cells grew in the subretinal space and invaded the choroid (Fig. 3G) and the episclera (Fig. 3H). Similar localization of IIA1.6-GFP cells was observed on frozen sections (Fig. 3H). The conventional B-cell surface markers CD19 and B220 (CD45R) and the MHC class II molecules were detected

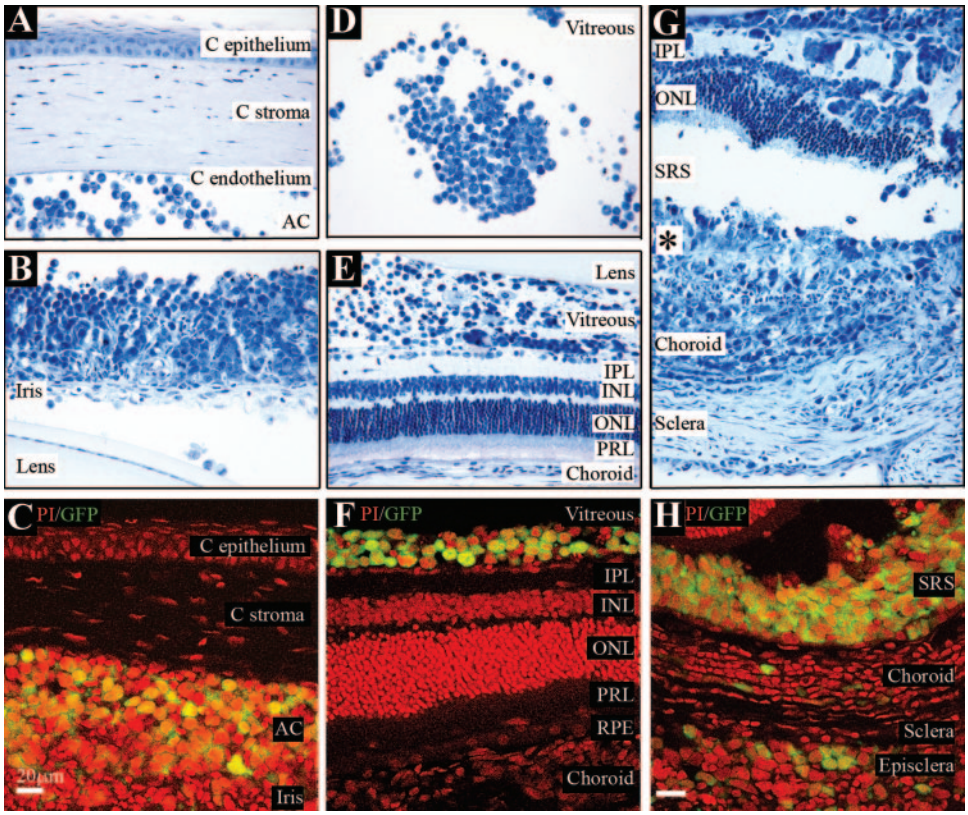

FIGURE 3. Ocular distribution of IIA1.6-GFP lymphoma B-cells after their intravitreous injection. Histologic aspect at day 12 of eyes injected with IIA1.6-GFP cells. Resin-embedded preparations counterstained with toluidine blue (**A**, **B**, **D**, **E**, **G**) and confocal microscopy on frozen sections counterstained in *red* with propidium iodide (**C**, **F**, **H**). Anterior segment infiltration by tumor cells: corneal endothelium (**A**), iris epithelium (**B**), and anterior chamber (**C**). Posterior segment infiltration by tumor cells: vitreous (**D**) and internal limiting membrane of the retina (**E**, **F**). Sections of the posterior segment of tumoral eyes (**G**, **H**) showing the retinal distribution of tumor cells in the IPL, the INL, and the OPL and a major disruption of ONL organization. Observation of tumor cells in the subretinal space (**G**, ✻; **H**, GFP cells at *top*), in the choroid and in the episclera (**H**). AC, anterior chamber; C, cornea; GCL, ganglion cell layer; INL, internal nuclear layer; IPL, internal plexiform layer; ONL, outer nuclear layer; OPL, outer plexiform layer; PI, propidium iodide; PRL, photoreceptor layer; RPE, retinal pigment epithelium; SRS, subretinal space; V, vitreous. Photographs are representative of similar sections from three eyes. Magnification: (**A**, **B**, **D**, **E**, **G**) ×25. Bars: (**C**, **F**, **H**) 20 μm.

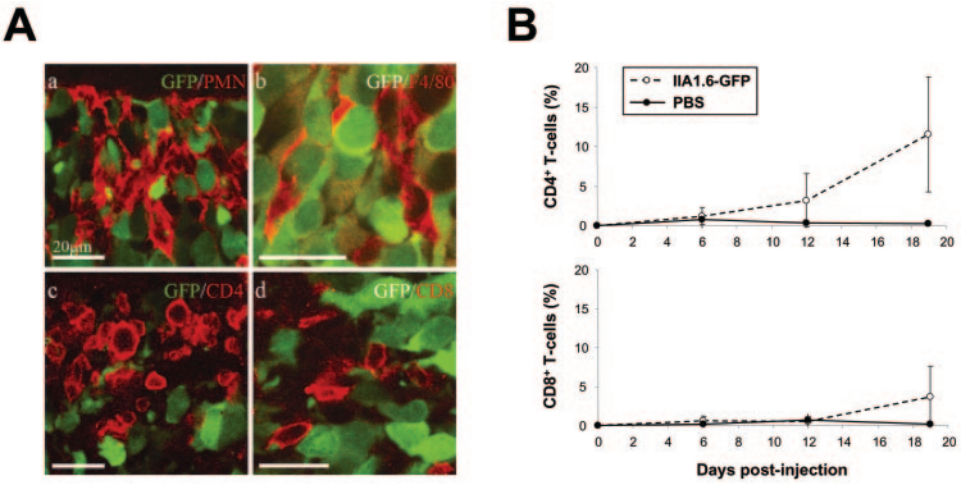

FIGURE 4. Phenotypic characterization of infiltrating cells. (**A**) Visualization by confocal microscopy of PMNs (**Aa**), F4/80$^+$ macrophages (**Ab**), CD4$^+$ T-lymphocytes (**Ac**), and CD8$^+$ T-lymphocytes (**Ad**). *Green*: IIA1.6-GFP tumor cells. Bars, 20 μm. (**B**) CD4$^+$ (*top*) or CD8$^+$ (*bottom*) T-cell infiltration at days 6, 12, and 19 determined by flow cytometric analysis as the percentage of CD4$^+$ or CD8$^+$ cells gated on CD3$^+$ T-cells, respectively, in the right eye injected at day 0 with PBS (n = 23) or 10^4 IIA1.6-GFP cells (n = 26). Data are from four independent experiments and standard deviations are represented.

in situ by immunohistochemistry in eyes injected with the GFP$^+$ tumor cells (Supplementary Fig. S1, online at http://www.iovs.org/cgi/content/full/48/7/3223/DC1).

Presence of T-Lymphocytes and Macrophages in the Tumor Microenvironment of Intraocular B-Cell Lymphoma

The various cellular subsets constitutive of the tumor microenvironment were studied by immunohistochemistry (Fig. 4A) and flow cytometric analysis (Fig. 4B). Immunohistochemical staining for polymorphonuclear neutrophils (PMNs), macrophages (F4/80), and T-lymphocytes (CD4, CD8) was performed on frozen sections at days 12 and 19. PMNs infiltrated the tumoral tissues from day 12 (data not shown) and were more abundant at day 19, especially in the choroid (Fig. 4Aa) and the anterior chamber. Similarly, F4/80-positive leukocytes were detected within the tumor at days 12 and 19 (Fig. 4Ab) and infiltrated the anterior chamber, the vitreous, the retina, the subretinal space and the choroid (Figs. 4Ac, 4Ad, respectively). According to flow cytometric analysis, they represented up to 10% of living cells (not shown). Few host B-cells were identified by flow cytometry or confocal microscopy as CD19$^+$GFP$^-$ cells (Fig. 1C and Supplementary Fig. S1, http://www.iovs.org/cgi/content/full/48/7/3223/DC1). In contrast, numerous CD4$^+$ and CD8$^+$ T-lymphocytes infiltrated the tumor at day 12 after injection. CD4$^+$ and CD8$^+$ T-lymphocytes were especially abundant in the choroid (Figs. 4Ac, 4Ad, respectively), the vitreous, and the anterior segment (data not shown), where they were in close contact with IIA1.6-GFP cells. The CD3$^+$ T-cell population represented more than 15% of living cells in the eyes. CD4$^+$ T-cells were the major subtype observed among CD3$^+$ T-cells, since they represent up to 10% of living cells (Fig. 4B). Thus, a robust immune cell infiltration in ocular lymphoma is observed from day 12 after intravitreal injection of IIA1.6-GFP cells. The other nontumoral cell populations were mainly composed of photoreceptor cells.

IL-10 Produced in the Tumor Microenvironment of Intraocular B-cell Lymphoma

Expression of IL-10 mRNAs was investigated by semiquantitative RT-PCR analysis performed on eyes after IIA1.6-GFP B-cells or PBS injection. The amount of the 455-bp product corresponding to the IL-10 mRNA, specifically amplified in the eyes injected with tumor cells, increased progressively between days 0 and 19. To assess the origin of IL-10, RT-PCR was performed, using mRNA from cultured IIA1.6-GFP cells, and revealed the presence of IL-10 mRNA (Fig. 5A). Presence of IL-10 in these cells grown in vitro was also confirmed by intracellular flow cytometric analysis (data not shown). To evaluate the IL-10 production at the protein level, IL-10 was measured by a cytometric bead array in the supernatant of cells from tumoral eyes (Fig. 5B). Ocular cells from the eyes injected with IIA1.6-GFP cells produced IL-10 in vitro, even in the absence of any stimulation. The level of IL-10 was only slightly modified after T-cell stimulation by anti-CD3$^+$ anti-CD28 mAbs, suggesting that IL-10 mainly originates from tumor cells and not from host T-cells. Cells from control eyes injected with PBS did not produce IL-10 at a detectable level.

Impaired Type 1 Pattern of Cytokine Expression in Intraocular Lymphoma

In the absence of any stimulation, supernatants of cultured cells extracted from tumoral eyes were assessed for cytokine production by cytometric bead array as shown in Figure 5B. TNFα and IFNγ were detected at significant levels showing a Th1-type polarization of TILs. However, IL-2 was undetectable, which renders the Th1-effector cells phenotype incomplete. After T-cell stimulation with anti-CD3$^+$ anti-CD28 mAbs, IFNγ was upregulated and IL-2 production was detected, displaying a complete Th1-type phenotype of these cells. A strong correlation was demonstrated between the level of IL-2 and IFN-γ, of IL-2 and TNFα, TNFα and IFNγ in the supernatant after stimulation, confirming the Th1/Tc1-type pattern of cytokine in tumoral eyes (Fig. 5C). However, even after stimulation, IL-12 could not be detected showing the absence of any Th1-type polarizing molecule in the supernatant. IL-4, the Th2-type cytokine, and Th2-polarizing factor were not significantly detected, even when cells were subjected to anti-CD3$^+$ anti-CD28 mAbs. IL-10, a Th2-type cytokine was detected at similar levels in stimulated and unstimulated cultures; its probable tumoral origin was discussed earlier. Thus, T-cells present in the tumor microenvironment seemed to be already polarized toward the Th1/Tc1 pattern. GM-CSF production was highly upregulated after T-cell stimulation, suggesting a possible functional cross-talk between T-cells and antigen-presenting cells already present in the tumor microenvironment.

To test the response to a proinflammatory signal, eye cells were stimulated by LPS in vitro. As expected, IL-6 production by ocular resident cells, obtained from PBS-injected eyes and by cells from IIA1.6-GFP-injected mice, was significantly upregulated compared to the unstimulated or anti-CD3$^+$ anti-CD28 mAb conditions. However, no IL-2, -4 or -12 was detected after LPS stimulation (data not shown).

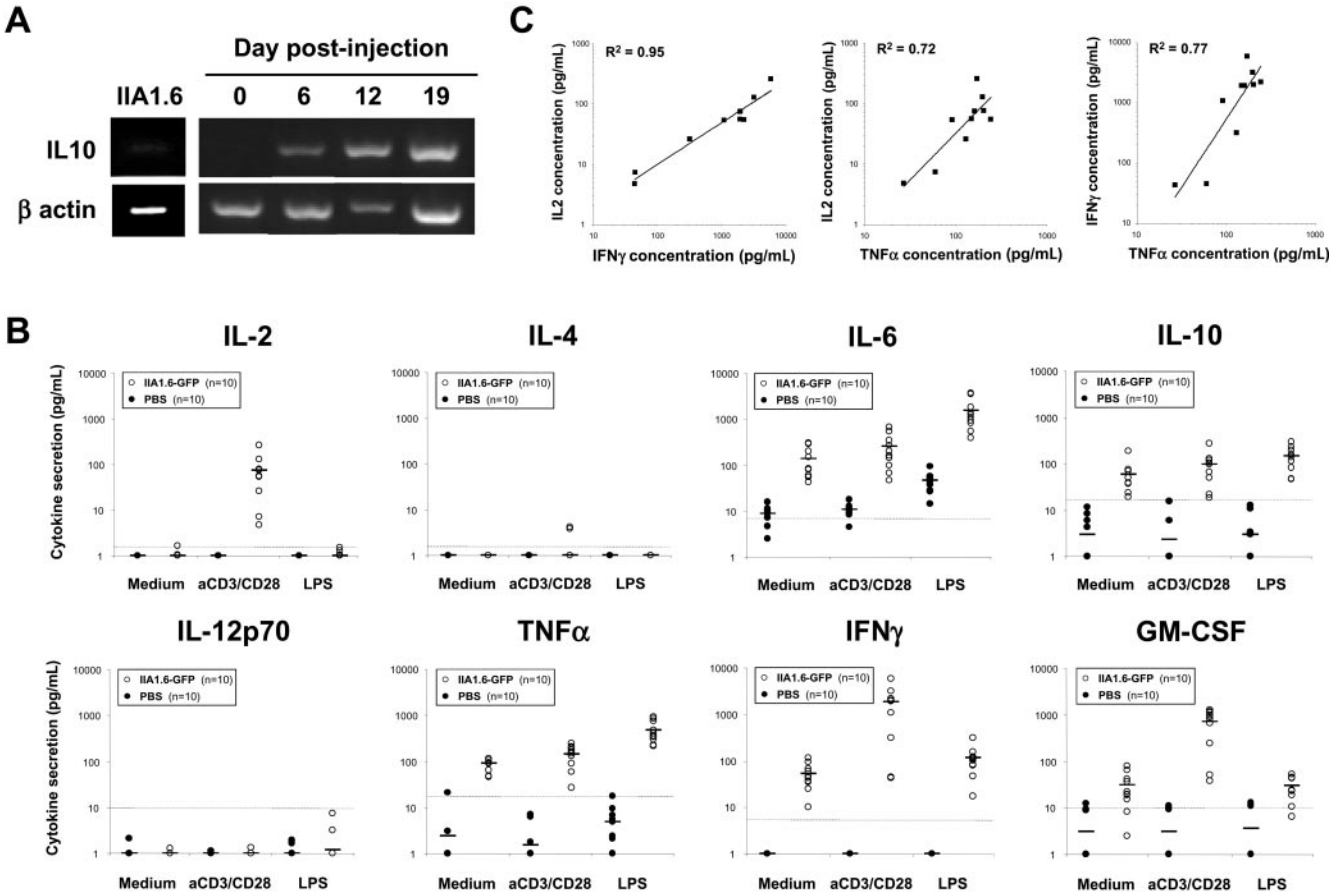

FIGURE 5. Cytokine profile in eyes with intraocular lymphoma and influence of T-cell stimulation on the cytokine secretion. (**A**) RT-PCR analysis for IL-10 mRNA expression of cultured IIA1.6-GFP cells or whole ocular cells obtained from eyes 6, 12, or 19 days after injection of 10^4 IIA1.6-GFP cells. (**B**) Ocular cells (10^4; obtained from PBS- or IIA1.6-GFP-injected eyes) were cultured in medium alone, or stimulated in vitro with anti-CD3 and -CD28 mAbs or with LPS. After 36 hours, culture supernatants were assayed for IL-2, IL-4, IL-6, IL-10, IL-12p70, IFNγ, TNFα, and GM-CSF with a cytometric bead assay. Each data point corresponds to the result in an individual eye ($n = 10$) and the *horizontal black bars* symbolize the mean of the respective results. *Dashed lines*: baseline of detection for each cytokine. Data are compiled from two independent experiments. (**C**) Correlation of IL-2, IFNγ, and TNFα secretion for total cells obtained from eyes intravitreally injected with 10^4 IIA1.6-GFP cells and in vitro stimulated with anti-CD3 and -CD28 mAbs. Each data point corresponds to the result from an individual eye ($n = 10$), and the line represents the regression curve.

DISCUSSION

The incidence of PCNSL has increased more than 10-fold over the past 10 years, and the incidence of PIOL, a subtype of PCNSL, has also increased, though more slowly, leading to an increasing concern regarding the diagnosis of this disease.[25–28] The lack of information concerning the pathogenesis of PIOL is due to the difficulties in studying this condition.[29] No cell line has been derived from human intraocular lymphoma cells, and the rare cells available from vitreous samples of PIOL patients are very fragile.[28,30] Moreover, the tumor microenvironment is difficult to study in vitreous samples. The present work describes the first murine model of intraocular B-cell lymphoma in immunocompetent mice. The development of intraocular lymphoma occurred in all eyes injected, demonstrating a highly reproducible model. At day 19 after injection of 10^4 lymphomatous B-cells, our experimental model closely mimics human PIOL, with vitreous, retinal, and anterior chamber infiltration by tumor cells and production of IL-10.[31]

It is accepted that the microenvironment plays a crucial role in the development of tumors. The cellular microenvironment displayed only a few endogenous B-lymphocytes in lymphomatous eyes. Thus, the local cellular antitumoral response seems to be mainly based on $CD3^+$ T-lymphocytes, which represents up to 12% of the living cells. The molecular microenvironment of PIOL was also studied in our model. Patients with PIOL usually display high levels of IL-10 and an increased IL-10 to IL-6 ratio in their aqueous humor or in the vitreous, which has been shown to aid in the diagnosis of PIOL.[31–33] The origin of this immunosuppressive cytokine is currently attributed to tumor cells. IL-10 may participate in the prevention of immune rejection of the tumor (as an anti-inflammatory cytokine) and in lymphomatous cell proliferation (as a B-cell growth factor).[34] In our model, IL-10 was detected in eyes bearing tumor. The level of IL-10 in tumoral eyes was only slightly modified after T-cell stimulation, suggesting that IL-10 mainly originates from tumor cells rather than infiltrating Th2 and/or Tr1 T-cells. This finding is highlighted by the detection of IL-10 in lymphomatous B cells in vitro. Increasing evidence suggests that a polarized T-cell response of TILs, of either the Th1 or Th2-type, can be involved in tumor immunity or in tumor tolerance.[16] A partial Th1 cytokine profile of TILs was observed in supernatants of cultured ocular cells in the absence of any stimulation, characterized by the production of IFNγ and TNFα, but the absence of IL-2. Th2-specific cytokines such as IL-4 were not detected in the tumoral eyes, with the exception of IL-10, which may result from secretion by tumor cells. After in vitro

stimulation of T-lymphocytes with anti-$CD3^+$ anti-CD28 antibodies, IL-2 production was induced, and IFNγ and GM-CSF were highly upregulated. Effector Th2 cytokines were still absent, since IL-4 level remained undetectable and IL-10 was only slightly upregulated. IL-12 and -4, required respectively for Th1 or Th2-polarization,[35] were undetectable in the supernatant of cultured cells, even after T-cell stimulation by anti-$CD3^+$ anti-CD28 mAbs. Thus, we hypothesize that the Th1/Tc1-type T-cells described earlier must have been polarized outside the eye, possibly in the draining lymph nodes. It has been shown that IL-10 exerts direct effects on human $CD4^+$ T-cell clones and on resting T-cells in peripheral blood, inducing specific inhibition of IL-2 production and proliferation.[36] This inhibitory effect of IL-10 could be an explanation of the status of partial inhibition of polarized TILs that we report in our model.

Altogether, these data suggest that TILs from intraocular B-lymphomas are characterized by a type-1 (Th1/Tc1-like) pattern of cytokine expression. This Th1/Tc1-like profile seems partially inhibited in vivo with a lack of IL-2 in the absence of any T-cell stimulation. These findings raise the possibility of an in situ T-cell immunostimulation to reactivate the Th1/Tc1 lymphocytes and improve the intraocular antitumoral immunity.

Acknowledgments

The authors thank Christophe Klein for confocal microscopy (Facility core of cellular imaging, Centre de Recherche des Cordeliers, Paris, France), Céline Terrada, Brice Geslot, Narimane Habour, and Sylvie Baudet for technical assistance and Nathalie Cassoux for helpful discussions.

References

1. Cassoux N, Merle-Beral H, Leblond V, et al. Ocular and central nervous system lymphoma: clinical features and diagnosis. *Ocul Immunol Inflamm*. 2000;8:243–250.
2. Cummings TJ, Stenzel TT, Klintworth G, Jaffe GJ. Primary intraocular T-cell-rich large B-cell lymphoma. *Arch Pathol Lab Med*. 2005; 129:1050–1053.
3. Galon J, Costes A, Sanchez-Cabo F, et al. Type, density, and location of immune cells within human colorectal tumors predict clinical outcome. *Science*. 2006;313:1960–1964.
4. Pages F, Berger A, Camus M, et al. Effector memory T cells, early metastasis, and survival in colorectal cancer. *N Engl J Med*. 2005; 353:2654–2666.
5. Dunn GP, Old LJ, Schreiber RD. The immunobiology of cancer immunosurveillance and immunoediting. *Immunity*. 2004;21: 137–148.
6. Zitvogel L, Tesniere A, Kroemer G. Cancer despite immunosurveillance: immunoselection and immunosubversion. *Nat Rev Immunol*. 2006;6:715–727.
7. Smyth MJ, Dunn GP, Schreiber RD. Cancer immunosurveillance and immunoediting: the roles of immunity in suppressing tumor development and shaping tumor immunogenicity. *Adv Immunol*. 2006;90:1–50.
8. Dunn GP, Old LJ, Schreiber RD. The three Es of cancer immunoediting. *Annu Rev Immunol*. 2004;22:329–360.
9. Dunn GP, Ikeda H, Bruce AT, et al. Interferon-gamma and cancer immunoediting. *Immunol Res*. 2005;32:231–245.
10. Beyer M, Schultze JL. Regulatory T cells in cancer. *Blood*. 2006; 108:804–811.
11. Wang RF. Regulatory T cells and innate immune regulation in tumor immunity. *Springer Semin Immunopathol*. 2006;28:17–23.
12. Tartour E, Fridman WH. Cytokines and cancer. *Int Rev Immunol*. 1998;16:683–704.
13. Li R, Ruttinger D, Li R, Si LS, Wang YL. Analysis of the immunological microenvironment at the tumor site in patients with non-small cell lung cancer. *Langenbecks Arch Surg*. 2003;388:406–412.
14. Angevin E, Kremer F, Gaudin C, Hercend T, Triebel F. Analysis of T-cell immune response in renal cell carcinoma: polarization to type 1-like differentiation pattern, clonal T-cell expansion and tumor-specific cytotoxicity. *Int J Cancer*. 1997;72:431–440.
15. Kidd P. Th1/Th2 balance: the hypothesis, its limitations, and implications for health and disease. *Altern Med Rev*. 2003;8:223–246.
16. Feili-Hariri M, Falkner DH, Morel PA. Polarization of naive T cells into Th1 or Th2 by distinct cytokine-driven murine dendritic cell populations: implications for immunotherapy. *J Leukoc Biol*. 2005;78:656–664.
17. Winter H, Hu HM, Poehlein CH, et al. Tumour-induced polarization of tumour vaccine-draining lymph node T cells to a type 1 cytokine profile predicts inherent strong immunogenicity of the tumour and correlates with therapeutic efficacy in adoptive transfer studies. *Immunology*. 2003;108:409–419.
18. Assaf N, Hasson T, Hoch-Marchaim H, et al. An experimental model for infiltration of malignant lymphoma to the eye and brain. *Virchows Arch*. 1997;431:459–467.
19. Chan CC, Fischette M, Shen D, Mahesh SP, Nussenblatt RB, Hochman J. Murine model of primary intraocular lymphoma. *Invest Ophthalmol Vis Sci*. 2005;46:415–419.
20. Li Z, Mahesh SP, Shen de F, et al. Eradication of tumor colonization and invasion by a B cell-specific immunotoxin in a murine model for human primary intraocular lymphoma. *Cancer Res*. 2006;66: 10586–10593.
21. Jones B, Tite JP, Janeway CA Jr. Different phenotypic variants of the mouse B cell tumor A20/2J are selected by antigen- and mitogen-triggered cytotoxicity of L3T4-positive, I-A-restricted T cell clones. *J Immunol*. 1986;136:348–356.
22. Jolly C, Jeanny JC, Behar-Cohen F, Laugier P, Saied A. High-resolution ultrasonography of subretinal structure and assessment of retina degeneration in rat. *Exp Eye Res*. 2005;81:592–601.
23. Pouvreau I, Zech JC, Thillaye-Goldenberg B, Naud MC, Van Rooijen N, de Kozak Y. Effect of macrophage depletion by liposomes containing dichloromethylene-diphosphonate on endotoxin-induced uveitis. *J Neuroimmunol*. 1998;86:171–181.
24. Thillaye-Goldenberg B, Goureau O, Naud MC, de Kozak Y. Delayed onset and decreased severity of experimental autoimmune uveoretinitis in mice lacking nitric oxide synthase type 2. *J Neuroimmunol*. 2000;110:31–44.
25. Rothova A, Ooijman F, Kerkhoff F, Van Der Lelij A, Lokhorst HM. Uveitis masquerade syndromes. *Ophthalmology*. 2001;108:386–399.
26. Tsai T, O'Brien JM. Masquerade syndromes: malignancies mimicking inflammation in the eye. *Int Ophthalmol Clin*. 2002;42:115–131.
27. Read RW, Zamir E, Rao NA. Neoplastic masquerade syndromes. *Surv Ophthalmol*. 2002;47:81–124.
28. Coupland SE, Bechrakis NE, Anastassiou G, et al. Evaluation of vitrectomy specimens and chorioretinal biopsies in the diagnosis of primary intraocular lymphoma in patients with masquerade syndrome. *Graefes Arch Clin Exp Ophthalmol*. 2003;241:860–870.
29. Johnston RL, Tufail A, Lightman S, et al. Retinal and choroidal biopsies are helpful in unclear uveitis of suspected infectious or malignant origin. *Ophthalmology*. 2004;111:522–528.
30. Rutzen AR, Ortega-Larrocea G, Dugel PU, et al. Clinicopathologic study of retinal and choroidal biopsies in intraocular inflammation. *Am J Ophthalmol*. 1995;119:597–611.
31. Merle-Beral H, Davi F, Cassoux N, et al. Biological diagnosis of primary intraocular lymphoma. *Br J Haematol*. 2004;124:469–473.
32. Tuaillon N, Chan CC. Molecular analysis of primary central nervous system and primary intraocular lymphomas. *Curr Mol Med*. 2001;1:259–272.
33. Chan CC. Molecular pathology of primary intraocular lymphoma. *Trans Am Ophthalmol Soc*. 2003;101:275–292.
34. Itoh K, Hirohata S. The role of IL-10 in human B cell activation, proliferation, and differentiation. *J Immunol*. 1995;154:4341–4350.
35. Trinchieri G. Interleukin-12 and the regulation of innate resistance and adaptive immunity. *Nat Rev Immunol*. 2003;3:133–146.
36. de Waal Malefyt R, Yssel H, de Vries JE. Direct effects of IL-10 on subsets of human CD4+ T cell clones and resting T cells: specific inhibition of IL-2 production and proliferation. *J Immunol*. 1993; 150:4754–4765.